Available online at www.sciencedirect.com
SCIENCE DIRECT®
Engineering Structures 26 (2004) 1261–1278
ENGINEERING STRUCTURES
www.elsevier.com/locate/engstruct

Performance estimates in seismically isolated bridge structures

Gordon P. Warn *, Andrew S. Whittaker

Department of Civil, Structural, and Environmental Engineering, University at Buffalo, Buffalo, NY 14260, USA

Received 8 September 2003; received in revised form 7 April 2004; accepted 12 April 2004

Abstract

An analytical study investigating the performance of seismically isolated bridge structures subjected to earthquake excitation is summarized. Here, performance is assessed using the following descriptors; maximum isolator displacement and energy demand imposed on individual seismic isolators. Nonlinear response-history analysis is employed considering 20 different isolation systems and three bins of earthquake ground motions. Results of these analyses are used to: (1) review the accuracy of the current AASHTO equation for the calculation of displacements in seismically isolated bridge structures, and (2) determine the increase in maximum horizontal displacement of a seismic isolator due to bidirectional seismic excitation, and (3) review the current AASHTO prototype testing requirements for seismic isolators under seismic loading conditions. The current AASHTO equation for calculating maximum isolator displacements is shown to underestimate median maximum horizontal displacements determined from bidirectional nonlinear response-history analysis. Maximum isolator displacements determined from bidirectional seismic excitation are shown to be significantly larger than those considering unidirectional seismic excitation. Two factors contributing to the increase in maximum isolator displacement are identified; additional displacement demand from a second (orthogonal) component, and the coupled response of seismic isolators. The current prototype testing requirements for seismic loading specified by the AASHTO are shown to result in energy demands that are inconsistent with those determined from numerical simulation of maximum earthquake excitation. An improved prototype testing protocol for seismic isolators subjected to seismic loading is proposed.

Keywords: Seismic isolator; Response-history analysis; Displacement; Energy demand; Prototype testing

1. Introduction

The key design variable for seismic isolation systems is displacement over the isolation interface. Isolator displacement dictates: (a) the space around the isolated superstructure to facilitate unrestricted movement of the superstructure, (b) the shear strain in elastomeric isolators and isolator stability, (c) the plan geometry of sliding isolators, and (d) forces transmitted to the bridge substructure for given isolator stiffness. Mechanical properties of the isolator assumed in the design and analysis of the isolation system are checked prior to fabrication of production seismic isolators and installation in the bridge structure through prototype testing.

The current design procedure for seismic isolation systems for bridge structures is set forth in the American Association of State Highway and Transportation Officials (AASHTO) Guide Specifications for Seismic Isolation Design [1]. The Guide Specifications provide procedures for the analysis of isolation systems, design of isolation systems and individual seismic isolators, and full-scale testing of seismic isolators. An estimate of the maximum displacement is calculated using a static-isolator (benchmark) calculation, Eq. (3) of the Uniform Load Method of the Guide Specifications. Eq. (3) (in SI units of millimeters) is presented here

$$d = \frac{250AS_iT_{\text{eff}}}{B} \tag{1}$$

where $250AS_i$ is the 5% damped spectral displacement corresponding to a 1-s period; T_{eff} is the effective period of the isolated structure at the design displacement in seconds; and B is a coefficient that modifies the spectrum for equivalent viscous damping other than 5%.

* Corresponding author. Tel.: +1-716-645-2114; fax: +1-716-645-3733.
E-mail address: warn@eng.buffalo.edu (G.P. Warn).

0141-0296/$ - see front matter © 2004 Elsevier Ltd. All rights reserved.
doi:10.1016/j.engstruct.2004.04.006

The 1-s spectral displacement is a function of the acceleration coefficient, A, and the site coefficient S_i. Values of A and S_i are given in Division 1-A: Seismic Design of the AASHTO Standard Specifications for Highway Bridges [2]. Eq. (1) assumes the effective period of the isolation system falls in the constant velocity portion of the design spectrum in which displacements are assumed to increase linearly with period.

Section 13.2 of the Guide Specifications include requirements for prototype testing of seismic isolators subjected to seismic loading, which include multiple cycles to the maximum design displacement, d. Specifically, the Guide Specifications in Section 13.2 write that a prototype isolator be subjected to: (a) three fully reversed cycles at the following multiples of the total design displacement: 1.0, 0.25, 0.5, 0.75, 1.0, 1.25, (b) not less than 10 and not more than 25 fully reversed cycles of loading at the design displacement, d, and (c) three fully reversed cycles of loading at the total design displacement. A maximum speed (frequency) for testing is not specified in the AASHTO specifications and therefore these tests are typically conducted at slow speeds. Accordingly, it is of significant import to bridge (and building) isolation construction that an estimate of maximum isolator displacement established using the procedures set forth in the AASHTO Guide Specifications be sufficiently accurate and that a prototype testing protocol be representative of the demand imposed on seismic isolators during a maximum earthquake.

Previous research has demonstrated that friction (F), friction-pendulum (FP) and lead-rubber (LR) isolation bearings exhibit a coupling between the response in each orthogonal direction [3–5]. Ignoring this coupling was shown to results in an underestimation of maximum isolator displacement by as much as 20% [3]. To capture the behavior of these seismic isolators under dynamic loading, the coupled behavior must be considered [3]. This research [3–5] also demonstrated that coupled plasticity, Bouc-Wen, and similar formulations are capable of predicting the response of seismic isolation systems composed of F, FP and LR isolators with reasonable accuracy.

The objectives of this research study are: (1) to review the accuracy of the current AASHTO equation for calculating displacements in seismically isolated bridge structures, and (2) to determine the increase in maximum isolator displacement due to bidirectional seismic excitation and to quantify the contribution due to the coupled behavior of the seismic isolators, and (3) to determine energy-related demands imposed on seismic isolators subjected to earthquake excitation and to translate these demands into a prototype testing protocol for seismic isolators subjected to seismic loading.

The results presented in this paper will form, in part, the basis for an improved equation to calculate displacements in isolated bridge structures. The new equation will build upon Eq. (1) and account for increases in displacement due to bidirectional excitation and the coupled response of F, FP and LR seismic isolators. The likely form of the new equation is:

$$d = \alpha_c \alpha_o \left[\frac{250 A S_i T_{\text{eff}}}{B}\right] \tag{2}$$

where α_c is a factor accounting for coupled response; α_o is a factor accounting for bidirectional excitation; and $250AS_iT_{\text{eff}}/B$ is the current AASHTO displacement equation.

For this study, response-history analysis was employed. A mathematical model of a simple seismically isolated bridge structure was developed and subjected to unidirectional and bidirectional earthquake excitation. Fig. 1 is a schematic of the isolated bridge,

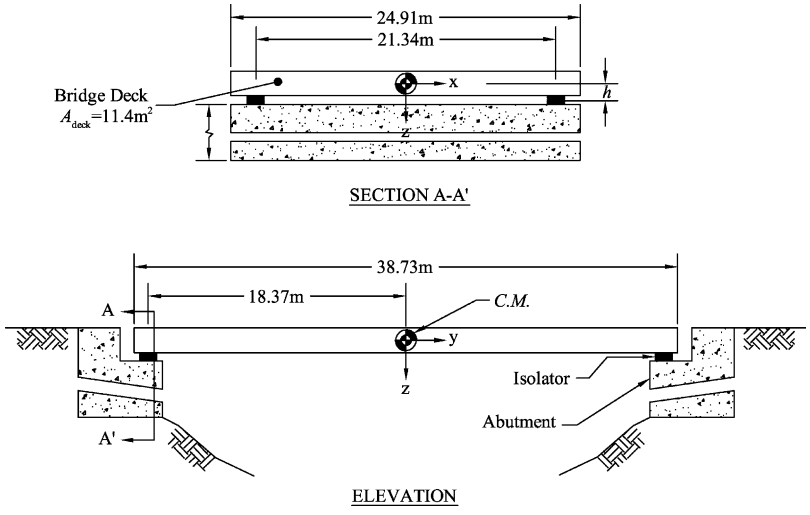

Fig. 1. Schematic of simple isolated bridge structure.

showing physical dimensions. The simplicity of the assumed bridge structure enables a clear understanding of the behavior of seismic isolation systems subjected to bidirectional earthquake excitation. The seismic isolators were idealized using a bilinear representation and modeled using a rate-independent coupled plasticity formulation [4,5]. Properties of the bilinear isolators, namely, Q_d the zero-displacement force-intercept and K_d the second-slope stiffness, were varied widely to ensure the results of this research were broadly applicable to seismically isolated bridge structures in the United States.

Response-history analysis was performed considering both unidirectional and bidirectional seismic excitation utilizing three bins of earthquake ground motions. Results of the response-history analyses were mined to determine maximum isolator displacements (displacement across the isolation interface). Maximum isolator displacement data were statistically sorted for each isolation system considered and used to review the accuracy of the current equation (Eq. (1)) for calculating displacements at the center of rigidity of an isolation system.

Maximum horizontal isolator displacement data determined from bidirectional response-history analysis were compared with maximum isolator displacements determined from unidirectional response-history analysis to determine the increase in maximum isolator displacement due to bidirectional excitation. Two factors contributing to the increase in maximum horizontal isolator displacement are identified. The first, demand from a second (orthogonal) component and the second, the coupled behavior exhibited by F, FP and LR seismic isolators. For this study, an empirical approach is employed due to the randomness of these effects on maximum isolator displacement. To identify (isolate) the contribution due to the coupling, the square-root-sum-of-squares (SRSS) response is calculated at each times step from the results of independent unidirectional response-history analyses using each component of a given ground motion pair. The SRSS response calculated in this manner is equivalent to bidirectional response-history analysis considering an uncoupled plasticity model (square yield function). Maximum isolator displacements determined from the SRSS response are compared with maximum isolator displacements determined from bidirectional response-history analysis considering a coupled plasticity model (circular yield function) to quantify the contribution of coupling to maximum isolator displacement.

Response data from the unidirectional and bidirectional response-history analyses performed in support of the maximum displacement study were mined to provide new knowledge related to the energy demands on seismic isolators and seismic isolation systems during a maximum earthquake. Energy demands were determined by numerically integrating the force–displacement response of individual seismic isolators obtained from response-history analysis. This information was used to review the current AASHTO prototype testing requirements for seismic isolators subjected to seismic loading [1] and to propose an improved prototype testing protocol for seismic isolators subjected to seismic loading.

2. Earthquake ground motions

2.1. Organization

A total of 72 pairs of earthquake ground motions were collected and organized into seven bins: an approach for organizing ground motions first proposed by Krawinkler [6]. Information on all seven bins is provided in Warn [7]. Three of these bins (32 pairs) and corresponding results are presented in this paper. Ground motions contained in these three bins represent levels of seismic hazard for which seismic isolation is typically employed. All but six pairs of the acceleration histories were extracted from two sources: the Pacific Earthquake Engineering Research (PEER) database [8] and the SAC Steel Project database [9]. Six ground motion pairs were obtained from Miranda [10].

The ground motion bins are denoted: (1) near-field, (2M) large magnitude, small distance, and (7) large magnitude, soft-soil. Ground motion components contained in Bins 1, 2M and 7 are presented in Tables 1, 2 and 3, respectively. Also presented in these tables is information such as event, moment magnitude, station, orientation, peak ground acceleration (PGA), distance-to-fault and site class and classification.

Bin 1 (near-field) contains 12 pairs of earthquake ground motions, 10 of which were extracted from the SAC Steel Project database [9]. The remaining two are from the 1999 Taiwan, Chi-Chi earthquake and were extracted from the PEER database [8]. Ground motions contained in Bin 1 represent large magnitude events with near-field characteristics and moment magnitude ranging from 6.7 to 7.6 in close proximity to the fault (distance-to-fault less than 10 km) and stiff soil site conditions (see Table 1). Eight of the 12 ground motion pairs contained in Bin 1 exhibited strong directivity effects, i.e., response from one component (fault normal) is significantly greater than the response from the orthogonal component (fault parallel) for periods greater than 1.0 s. The first 10 pairs of ground motions listed in Table 1 were classified with a soil type D as designated by the National Earthquake Hazard Reduction Program [11] corresponding to a stiff soil profile (average shear wave velocity ranging from 180 to 360 m/s). The remaining two pairs of ground motions listed in Table 1 were classified with a soil type

Table 1
Near-field ground motions (Bin 1)

Record	Event	Year	Moment magnitude	Station	Orientation	PGA (g)	Distance-to-fault (km)	Site class/ classification
NF01	Tabas, Iran	1978	7.4	Tabas	FN	0.90	1.2	D/NEHRP[a]
NF02	Tabas, Iran	1978	7.4	Tabas	FP	0.98	1.2	D/NEHRP[a]
NF03	Loma Prieta	1989	7.0	Los Gatos	FN	0.72	3.5	D/NEHRP[a]
NF04	Loma Prieta	1989	7.0	Los Gatos	FP	0.46	3.5	D/NEHRP[a]
NF05	Loma Prieta	1989	7.0	Lex Dam	FN	0.69	6.3	D/NEHRP[a]
NF06	Loma Prieta	1989	7.0	Lex Dam	FP	0.37	6.3	D/NEHRP[a]
NF07	Cape Mendocino	1992	7.1	Petrolia	FN	0.64	8.5	D/NEHRP[a]
NF08	Cape Mendocino	1992	7.1	Petrolia	FP	0.65	8.5	D/NEHRP[a]
NF09	Erzincan, Turkey	1992	6.7	Erzincan	FN	0.43	2	D/NEHRP[a]
NF10	Erzincan, Turkey	1992	6.7	Erzincan	FP	0.46	2	D/NEHRP[a]
NF11	Landers	1992	7.3	Luceme	FN	0.71	1.1	D/NEHRP[a]
NF12	Landers	1992	7.3	Luceme	FP	0.80	1.1	D/NEHRP[a]
NF13	Northridge	1994	6.7	Rinaldi	FN	0.89	7.5	D/NEHRP[a]
NF14	Northridge	1994	6.7	Rinaldi	FP	0.39	7.5	D/NEHRP[a]
NF15	Northridge	1994	6.7	Olive View	FN	0.73	6.4	D/NEHRP[a]
NF16	Northridge	1994	6.7	Olive View	FP	0.60	6.4	D/NEHRP[a]
NF17	Kobe	1995	6.9	JMA	FN	1.09	3.4	D/NEHRP[a]
NF18	Kobe	1995	6.9	JMA	FP	0.57	3.4	D/NEHRP[a]
NF19	Kobe	1995	6.9	Takatori	FN	0.79	4.3	D/NEHRP[a]
NF20	Kobe	1995	6.9	Takatori	FP	0.42	4.3	D/NEHRP[a]
TCU065-W	Chi-Chi, Taiwan	1999	7.6	TCU065	West	0.81	0.98	C/USGS
TCU065-N	Chi-Chi, Taiwan	1999	7.6	TCU065	North	0.60	0.98	C/USGS
TCU075-W	Chi-Chi, Taiwan	1999	7.6	TCU075	West	0.33	1.49	C/USGS
TCU075-N	Chi-Chi, Taiwan	1999	7.6	TCU075	North	0.26	1.49	C/USGS

[a] Average shear wave velocity ranging from 180 to 360 m/s.

C designated by the United States Geological Survey (USGS) corresponding to a stiff soil profile (average shear wave velocity ranging from 180 to 360 m/s) [8].

Ground motion pairs contained in Bin 2M represent large magnitude events with moment magnitude ranging from 6.9 to 7.4, distance-to-fault ranging from 10 to 30 km and stiff soil or rock site conditions (see Table 2). Ground motions contained in Bin 2M exhibit no clear directivity effects and were classified with soil type A, B or C as designated by the USGS soil classification corresponding to rock (average shear wave velocity > 750 m/s), very dense soil or soft-rock (average shear wave velocity ranging from 360 to 750 m/s) and stiff soil (average shear wave velocity ranging from 180 to 360 m/s), respectively.

Bin 7 is comprised of ground motions representing large magnitude events with moment magnitude ranging from 6.9 to 8.1 and soft-soil site conditions (see Table 3). Due to the limited number of large magnitude, soft-soil records distance-to-fault criteria was relaxed. The first four pairs of ground motions are classified as either E or F as per the NEHRP designation based on descriptions of local soil geology [12,13]. Site class E represents soil profiles with soft clay layers greater than 3 m in depth (average shear wave velocity < 180 m/s) [11]. Site class F represents soil profiles with soft organic clay layers greater than 3 m in depth or soft clay layers with depth greater than 36 m [11]. Ground motion components from the 1989 Loma Prieta earthquake, San Francisco International Airport station, shown in Table 3 were assigned site class C as per the USGS designation based on the information provided in a ground motion database [8], but the local geology was described by Miranda as "Bay Mud" [13]. Site class C as per the USGS represents soil profiles with an average shear wave velocity ranging from 180 to 360 m/s. Ground motion records from the 1999 Kocaeli, Turkey earthquake, Duzce and Yarimca stations also shown in Table 3 were assigned site class C as per the USGS designation based on the information provided in a ground motion database [8], but another source describes the local geology for these stations as "soft-soil" [14]. The remaining three pairs of ground motions contained in Bin 7 are classified as D as per the USGS designation with average shear wave velocities less than 180 m/s, respectively [8].

2.2. Spectral demand

Response spectra were generated for each ground motion component used in this study. All spectra were generated for 5% critical damping. A goodness-of-fit test was conducted on several samples of spectral acceleration data for various periods considering two continuous probability distribution functions, the normal

Table 2
Large magnitude, small distance ground motions (Bin 2M)

Record	Event	Year	Moment magnitude	Station	Orientation	PGA (g)	Distance-to-fault (km)	Site class/ classification
G01000	Loma Prieta	1989	6.9	Gilroy Array #1 47379	0	0.41	11.2	A/USGS[a]
G01090	Loma Prieta	1989	6.9	Gilroy Array #1 47379	90	0.47	11.2	A/USGS[a]
GBZ000	Kocacli, Turkey	1999	7.4	Gebze	0	0.24	17	A/USGS[a]
GBZ270	Kocacli, Turkey	1999	7.4	Gebze	270	0.14	17	A/USGS[a]
STG000	Loma Prieta	1989	6.9	58065 Saratoga Aloha Ave	0	0.51	13	B/USGS[b]
STG090	Loma Prieta	1989	6.9	58065 Saratoga Aloha Ave	90	0.32	13	B/USGS[b]
RIO270	Cape Mendocino	1992	7.1	89324 Rio Dell Over Pass FF	270	0.39	18.5	B/USGS[b]
RIO360	Cape Mendocino	1992	7.1	89324 Rio Dell Over Pass FF	360	0.55	18.5	B/USGS[b]
JOS000	Landers	1992	7.3	22170 Joshua Tree	0	0.27	11.6	B/USGS[b]
JOS090	Landers	1992	7.3	22170 Joshua Tree	90	0.28	11.6	B/USGS[b]
G02000	Loma Prieta	1989	6.9	47380 Gilroy Array #2	0	0.37	12.7	C/USGS[c]
G02090	Loma Prieta	1989	6.9	47380 Gilroy Array #2	90	0.32	12.7	C/USGS[c]
YER270	Landers	1992	7.3	22074 Yermo Fire Station	270	0.25	24.9	C/USGS[c]
YER360	Landers	1992	7.3	22074 Yermo Fire Station	360	0.15	24.9	C/USGS[c]
ABN000	Kobe	1995	6.9	Abeno	0	0.22	23.8	C/USGS[c]
ABN090	Kobe	1995	6.9	Abeno	90	0.24	23.8	C/USGS[c]
BOL000	Duzce, Turkey	1999	7.1	Bolu	0	0.73	17.6	C/USGS[c]
BOL090	Duzce, Turkey	1999	7.1	Bolu	90	0.82	17.6	C/USGS[c]
CNP106	Northridge	1994	6.7	90053 Canoga Park Topanga Can	106	0.36	15.8	C/USGS[c]
CNP196	Northridge	1994	6.7	90053 Canoga Park Topanga Can	196	0.42	15.8	C/USGS[c]

[a] Average shear wave velocity greater than 750 m/s.
[b] Average shear wave velocity ranging from 360 to 750 m/s.
[c] Average shear wave velocity ranging from 180 to 360 m/s.

(or Gaussian) and the lognormal distributions. From this investigation, it was determined that a lognormal distribution better characterized the distribution of spectral acceleration data [7]. Therefore, the seismic hazard for each bin is characterized using the median of all spectra. Median spectra were determined using the sample mean and sample standard deviation of the logarithm of the spectral acceleration data.

Median, 84th percentile and 16th percentile acceleration response spectra calculated for ground motion Bins 1, 2M and 7 are shown in Figs. 2a,b and c, respectively. Eighty-fourth and 16th percentile spectra are shown to provide information on the variability of the spectral acceleration data. Median short period spectral accelerations (0.2 s) were determined to be 1.0 g, 0.71 g and 0.37 g for Bins 1, 2M and 7, respectively. Median 1-s spectral accelerations were determined to be 0.83 g, 0.36 g and 0.30 g for Bins 1, 2M, and 7, respectively. For this study, the median 1-s spectral accelerations were used to calculate the design displacement of the simple isolated bridge using the AASHTO Uniform Load Method [1].

The median spectrum for each bin represents a null directivity spectrum with the exception of Bin 1 where component orientation with respect to the fault has been preserved in approximate fault normal and fault parallel orientation. The first (larger) component of each of the ground motion pairs was assumed to lie in the fault normal orientation. Equivalently, the second (smaller) components were assumed to lie in approximate fault parallel orientation. Shown in Fig. 3 are median first component, median second component and median of all component acceleration response spectra. From Fig. 3, it is observed that the median first component spectrum lies significantly above the median second component spectrum. Median first component short period (0.2 s) and 1-s spectral accelerations were determined to be 1.0 g and 1.26 g, respectively.

3. Modeling

3.1. Simple bridge model

A mathematical model of a simple isolated bridge structure was assumed for nonlinear response-history analysis. This model represents the simplest of isolated

Table 3
Large magnitude, soft-soil ground motions (Bin 7)

Record	Event	Year	Moment magnitude	Station	Orientation	PGA (g)	Distance-to-fault (km)	Site class/ classification
SCT19seew	Mexico City	1985	8.1	SCT	EW	0.17	385	E/NEHRP[a]
SCT19sens	Mexico City	1985	8.1	SCT	NS	0.10	385	E/NEHRP[a]
MEN270	Loma Prieta	1989	6.9	1515 Forster City—355 Menhaden	270	0.11	51.2	F/NEHRP[b]
MEN360	Loma Prieta	1989	6.9	1515 Forster City—355 Menhaden	360	0.12	51.2	F/NEHRP[b]
EMV260	Loma Prieta	1989	6.9	Emeryville	260	0.24	96	F/NEHRP[b]
EMV350	Loma Prieta	1989	6.9	Emeryville	350	0.21	96	F/NEHRP[b]
OHW035	Loma Prieta	1989	6.9	Oakland (Outer Harbor Wharf)	35	0.29	76	F/NEHRP[b]
OHW305	Loma Prieta	1989	6.9	Oakland (Outer Harbor Wharf)	305	0.27	76	F/NEHRP[b]
RWC043	Loma Prieta	1989	6.9	Redwood City	43	0.28	47.9	D/USGS[a]
RWC233	Loma Prieta	1989	6.9	Redwood City	233	0.23	47.9	D/USGS[a]
SFA000	Loma Prieta	1989	6.9	S.F. International Airport	0	0.24	64.4	C/USGS[c,d]
SFA090	Loma Prieta	1989	6.9	S.F. International Airport	90	0.33	64.4	C/USGS[c,d]
TRI000	Loma Prieta	1989	6.9	Treasure Island (Fire Station)	0	0.10	82.9	D/USGS[a]
TRI090	Loma Prieta	1989	6.9	Treasure Island (Fire Station)	90	0.16	82.9	D/USGS[a]
ATS000	Turkey, Kocacli	1999	7.4	Ambarli Termik Santrali	0	0.25	78.9	C/USGS[a]
ATS090	Turkey, Kocacli	1999	7.4	Ambarli Termik Santrali	90	0.19	78.9	USGS[c,e]
DZC180	Turkey, Kocacli	1999	7.4	Duzce	180	0.31	12.7	USGS[c,e]
DZC270	Turkey, Kocacli	1999	7.4	Duzce	270	0.36	12.7	USGS[c,e]
YPT060	Turkey, Kocacli	1999	7.4	Yarimca	60	0.27	2.6	USGS[c,e]
YPT330	Turkey, Kocacli	1999	7.4	Yarimca	330	0.35	2.6	USGS[c,e]

[a] Average shear wave velocity less than 180 m/s.
[b] Soil profile containing soft organic clay layers or thick clay layers.
[c] Average shear wave velocity ranging from 180 to 360 m/s.
[d] Site class and classification obtained from ground motion database [8], site classification of "soft-soil" as per [14].
[e] Site class and classification obtained from ground motion database [8], local geology of "Bay Mud" as per [13].

bridge structures and assumes both the superstructure and substructure to be rigid (see Fig. 1). The simplicity of this bridge model enables a clear understanding of the effect of bidirectional excitation on the response of isolation systems modeled using a coupled plasticity formulation.

Physical properties of the single-span superstructure were based on the middle span of a three-span example bridge structure set forth in a report by the Applied Technology Council (ATC) [15]. The bridge deck was assumed to be concrete with density equal to 2300 kg/m^3 resulting in a total deck weight of approximately 9900 kN. Each of the four seismic isolators is assumed to carry one quarter of the total deck weight (2475 kN). The center of mass (denoted C.M. in Fig. 1) is assumed to coincide with the center of rigidity of the isolation system in both horizontal and vertical planes, eliminating torsion and overturning moment caused by inertial forces.

3.2. Plasticity model

The seismic isolators were modeled using a rate-independent coupled plasticity model [4,5]. Parameters used for the coupled plasticity model are based on a bilinear characterization of the seismic isolators. This bilinear characterization and defining parameters are shown in Fig. 4. Here, Q_d is the zero-displacement force-intercept; F_y is the yield force; K_u is the elastic stiffness; K_d is the second-slope stiffness; K_{eff} is the effective stiffness (peak-to-peak); d_y is the yield displacement assumed to be 0.025 cm for all isolation systems considered (typical of FP isolation bearings); $d_{\max}$ is the maximum displacement; and EDC is the energy dissipated in one fully reversed cycle to the maximum displacement shown by the area within the force–displacement loop. Note this characterization is the same as that assumed by the AASHTO Guide Specifications for Seismic Isolation Design [1].

For two-dimensional analysis, the restoring force of the seismic isolator subjected to lateral displacement is determined as

$$\begin{bmatrix} F_x \\ F_y \end{bmatrix} = \begin{bmatrix} F_{px} \\ F_{py} \end{bmatrix} + \begin{bmatrix} K_d & 0 \\ 0 & K_d \end{bmatrix} \begin{bmatrix} u_x \\ u_y \end{bmatrix} \tag{3}$$

where F_x and F_y are components of the restoring force in the x- and y-horizontal directions, respectively; F_{px} and F_{py} are components of the plastic force in the x- and y-horizontal directions, respectively; K_d is the second-slope stiffness; and u_x and u_y are displacements

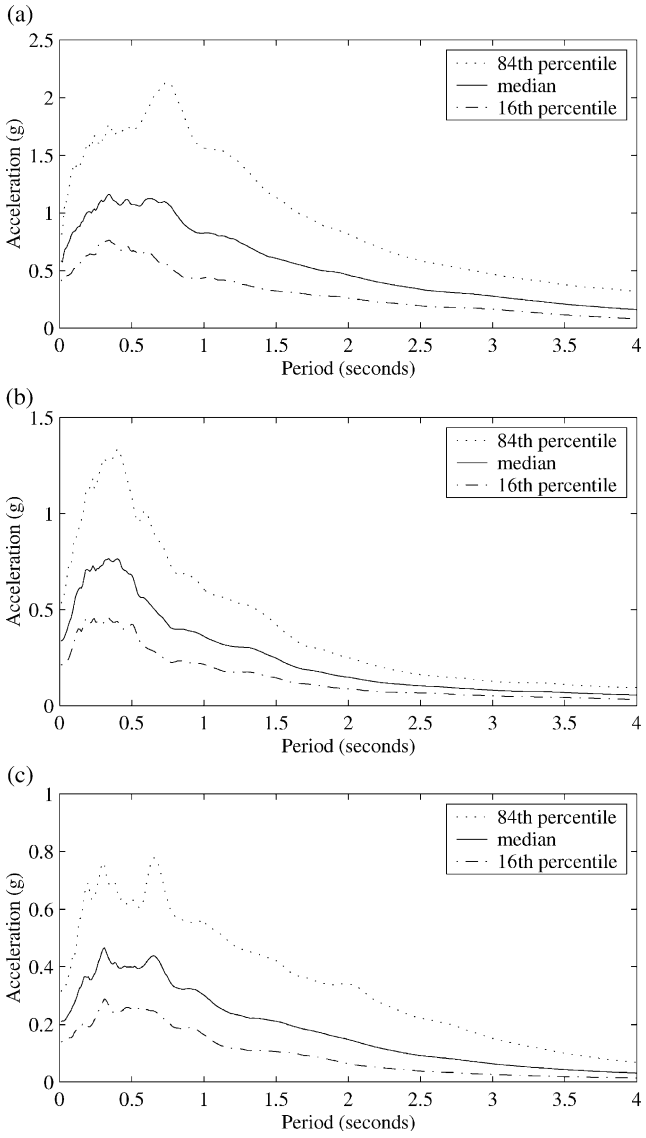

Fig. 2. Median, 16th and 84th percentile elastic, 5% damped, absolute acceleration response spectra: (a) Bin 1; (b) Bin 2M; (c) Bin 7.

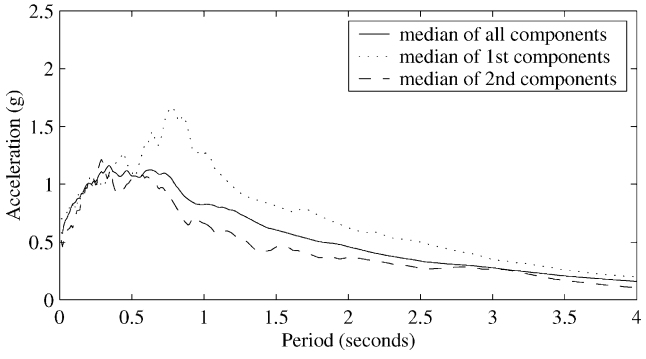

Fig. 3. Median elastic, 5% damped, absolute acceleration spectra for all components, 1st components, and 2nd components of Bin 1 ground motion pairs.

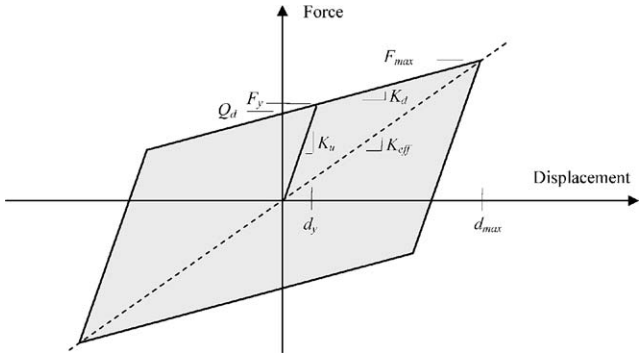

Fig. 4. Bilinear force–displacement characterization of an isolation bearing.

in the x- and y-horizontal directions, respectively. The components of the plastic force, F_{px} and F_{py}, are determined based on the assumed circular yield function with magnitude given by

$$F_p = \sqrt{F_{px}^2 + F_{py}^2} \tag{4}$$

where F_p is the plastic force magnitude (radius of circular yield function) that is constant. The plastic force magnitude corresponds to the strength of the lead core in a LR bearing that is estimated from the yield strength of the lead and the cross-sectional area of the lead core, $\sigma_L A_L$, or the friction force (assuming Coulomb friction) in a FP bearing, which is calculated as the dynamic coefficient of friction multiplied by the weight acting on the isolator, μW.

The difference between a coupled (circular yield function) and an uncoupled (square yield function) plasticity formulation is demonstrated by comparing the response of each model to a predefined (hourglass shaped) displacement orbit, shown in Fig. 5. Shown in Fig. 5a is the hourglass shaped displacement orbit. This presentation is similar to that introduced by previous researchers [4,5]. For each model, the force orbit, x-direction force–displacement response and y-direction force–displacement response are shown in Figs. 5b, c and d, respectively, where the response of the coupled plasticity model is indicated by a solid line and the response of the uncoupled model by a dashed-dot line. The displacement orbit and corresponding response of the coupled model are annotated to indicate common points in the response-history. Figs. 5c and d clearly show the effect the coupled behavior has on the unidirectional response of the isolation system: (1) the decrease in the effective stiffness (peak-to-peak stiffness) and (2) the reduction in the effective damping, which is defined [1] to be

$$\beta_{eff} = \frac{EDC}{2\pi K_{eff} d^2} \tag{5}$$

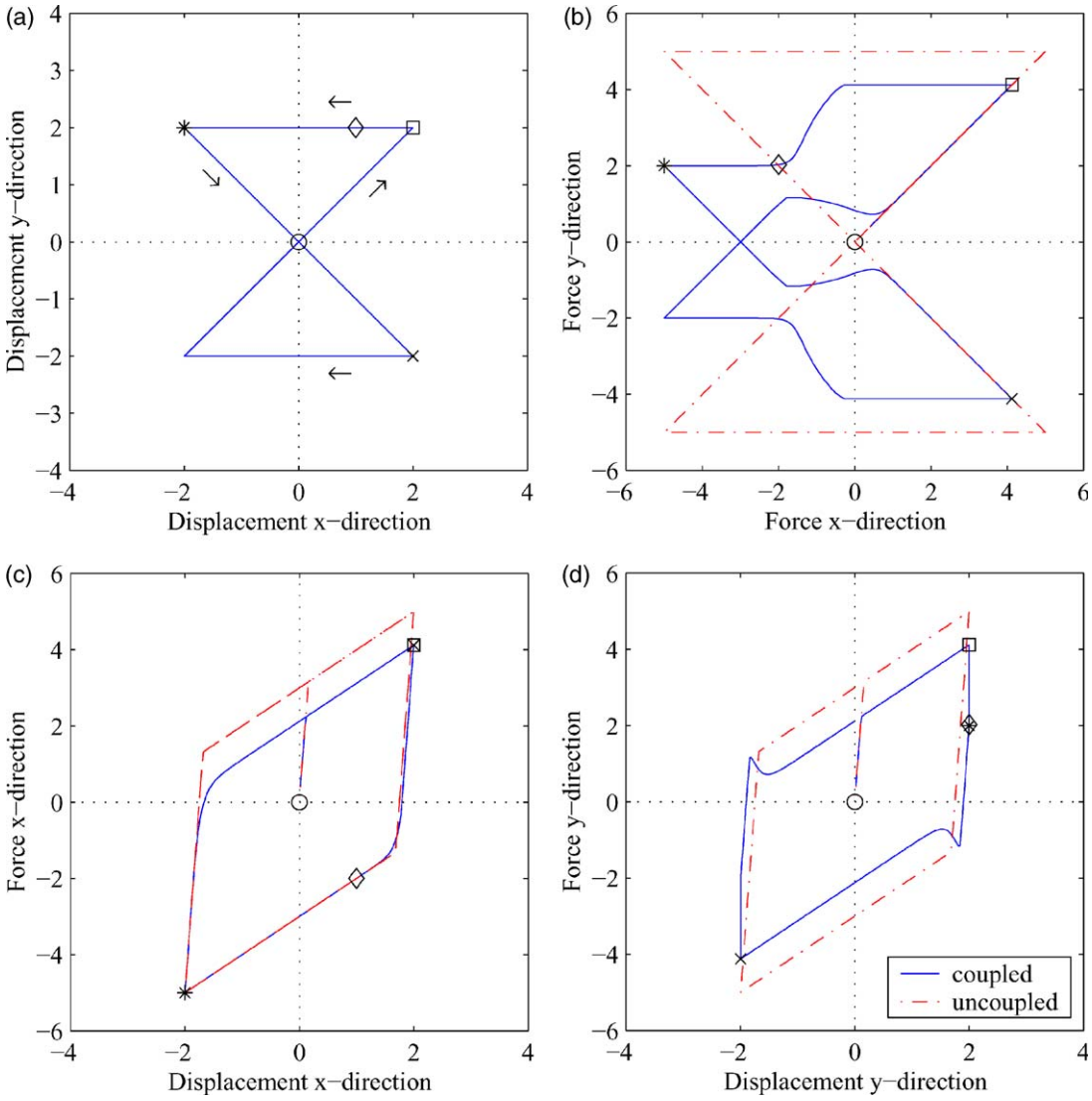

Fig. 5. Comparison of the response of a coupled and an uncoupled plasticity model subjected to an hourglass shaped displacement orbit: (a) displacement orbit; (b) force orbit; (c) x-direction force–displacement loop; (d) y-direction force–displacement loop.

where d is the displacement of the isolator. This reduction in effective stiffness and effective damping translate to an increase in maximum isolator displacement during numerical simulation of earthquake excitation. However, the magnitude of the increase in displacement depends on the plastic force magnitude and the phasing of the orthogonal earthquake ground motion components. Because the phase of earthquake ground motion components is random, the resulting increase in displacement is also random.

3.3. Equations of motion

The dynamic behavior of the simple bridge model is described using two degrees of freedom, namely, translation in the x- and y-directions at the center of rigidity (center of mass) and is

$$\begin{bmatrix} m_{\text{deck}} & 0 \\ 0 & m_{\text{deck}} \end{bmatrix} \begin{bmatrix} \ddot{u}_x(t) \\ \ddot{u}_y(t) \end{bmatrix} + \begin{bmatrix} c & 0 \\ 0 & c \end{bmatrix} \begin{bmatrix} \dot{u}_x(t) \\ \dot{u}_y(t) \end{bmatrix} + \begin{bmatrix} F_x(t) \\ F_y(t) \end{bmatrix} = -1 \begin{bmatrix} m_{\text{deck}} & 0 \\ 0 & m_{\text{deck}} \end{bmatrix} \begin{bmatrix} \ddot{u}_{gx}(t) \\ \ddot{u}_{gy}(t) \end{bmatrix} \tag{6}$$

where m_{deck} is the mass of the bridge deck; c is the assumed viscous damping constant of the bridge superstructure assumed to be equal to zero; $\ddot{u}_x(t)$ and $\ddot{u}_y(t)$ are components of the acceleration response in the x- and y-directions, respectively; $\dot{u}_x(t)$ and $\dot{u}_y(t)$ are components of the velocity response in the x- and y-directions, respectively; and $F_x(t)$ and $F_y(t)$ are components of the isolator restoring force in the x- and y-directions, respectively.

The equation of motion shown in Eq. (6) was integrated numerically using Newmark's step-by-step integration procedure [16]. Because the assumed force–displacement relationship for the seismic isolators is nonlinear (bilinear), an iterative procedure is required at each time step. A modified Newton–Raphson procedure is used to determine the restoring force at each time step during the solution procedure. This solution procedure is implicit and unconditionally stable due to the choice of integration parameters, $\gamma = 1/2$ and $\beta = 1/4$ [16].

Displacement and force results obtained from unidirectional response-history analysis considering three isolation systems and one ground motion pair using the previously mentioned numerical procedure implemented in Matlab [17] were verified using a commercially available structural analysis software package, SAP2000 Nonlinear [18]. An identical mathematical model was generated in SAP2000. Results from the SAP analyses agreed exceptionally well with the results obtained from the Matlab code [7].

3.4. Isolation systems considered and response-history analysis

Isolator parameters, specifically, Q_d (zero-displacement force-intercept) and T_d (second-slope period), were varied widely to ensure the results of this study were applicable to the design of isolation systems in the United States. Twenty isolation systems were considered with T_d ranging from 1.5 to 4.0 s and Q_d/W (zero-displacement force-intercept normalized by the weight acting on the isolator) ranging from 0.03 to 0.12. We note that the second-slope period is related to the second-slope stiffness (K_d) through the following expression

$$T_d = 2\pi\sqrt{\frac{W}{K_d g}} \tag{7}$$

where W is the weight acting on an individual isolator; and g is the gravitational acceleration constant. Table 4 shows the range of isolator parameters considered. In this table, each isolation system is identified using a three digit alpha-numeric naming system. For example, S33 denotes an isolation system with $Q_d/W = 0.09$ and $T_d = 2.5$ s. Typical bridge isolation systems are shown by the shaded region of the systems matrix in Table 4, where Q_d/W ranges from 0.06 to 0.12 and T_d from 2.0 to 3.0 s.

Table 4
Isolator parameter matrix

		T_d (s)				
		1.5	2.0	2.5	3.0	4.0
Q_d/W	0.03	S11	S12	S13	S14	S15
	0.06	S21	S22	S23	S24	S25
	0.09	S31	S32	S33	S34	S35
	0.12	S41	S42	S43	S44	S45

4. Displacement estimates

4.1. Static analysis procedure (AASHTO calculation)

Maximum isolator displacements were calculated using the AASHTO Uniform Load Method (Eq. (1)) for each isolation system utilizing the median 1-s spectral acceleration for each ground motion bin. For this calculation, the median 1-s spectral acceleration was assumed to be equal to AS_i, the product of the acceleration coefficient (A) and the site coefficient (S_i). Values of the damping coefficient (B) were determined from Table 7.1-1 of the AASHTO Guide Specifications [1]. Results of the AASHTO calculation, namely, isolator displacements (d), are plotted in Fig. 6 for each of the 20 isolation systems and three ground motion bins. In this figure, isolator displacements are plotted as a function of the effective period (T_{eff}).

4.2. Unidirectional response-history analysis

The results of unidirectional response-history analysis were mined to determine maximum isolator displacements. Maximum isolator displacements were statistically sorted for each isolation system and compared with isolator displacements determined from the AASHTO calculation. Shown in Fig. 7 is a comparison of the AASHTO calculation with median maximum isolator displacements determined from unidirectional response-history analysis for each of the three ground motion bins. In each of these plots, the horizontal axis represents the AASHTO calculated displacement, denoted d, in units of cm. The vertical axis represents the median maximum isolator displacement determined from unidirectional response-history analysis, denoted d_x, in units of cm. Also plotted is a line with slope equal to one for reference. From Fig. 7a, it is observed that the AASHTO calculation predicts the median maximum isolator displacements for Bin 1 (near-field) reasonably well but slightly underestimates the median maximum isolator displacement for a few systems with Q_d/W equal to 0.03, 0.06, and 0.09. The maximum difference (d_x/d) is observed to be 1.23. From Fig. 7b (Bin 2M), the AASHTO calculation is observed to conservatively predict the maximum isolator displacements determined from unidirectional response-history analysis for all 20 isolation systems. Fig. 7c (Bin 7) shows the AASHTO calculation conservatively estimates the median maximum isolator displacement for all isolation systems with Q_d/W equal to 0.09 and 0.12 and for isolation systems with $Q_d/W \leq 0.06$ and $T_d \geq 3.0$ s. However, the AASHTO calculation is observed to underestimate the median maximum

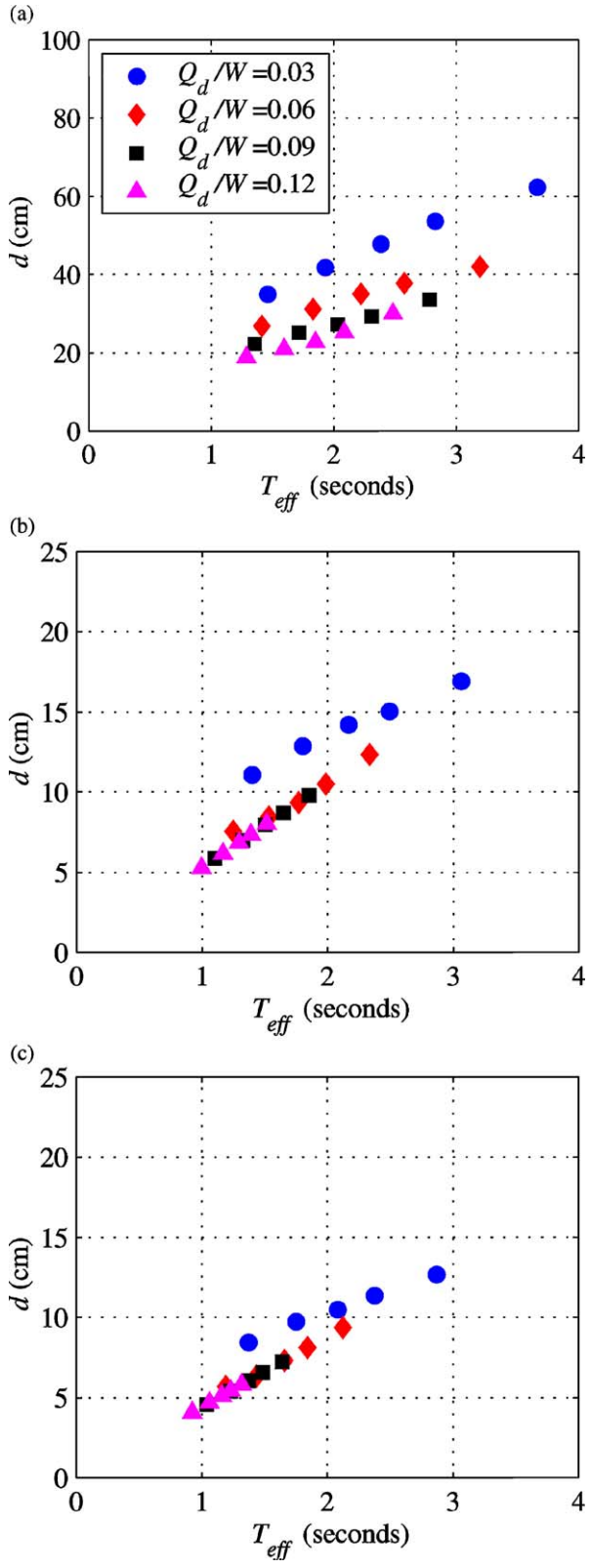

Fig. 6. Maximum isolator displacements calculated using Eq. (3b) of the AASHTO Uniform Load Method: (a) Bin 1; (b) Bin 2M; (c) Bin 7.

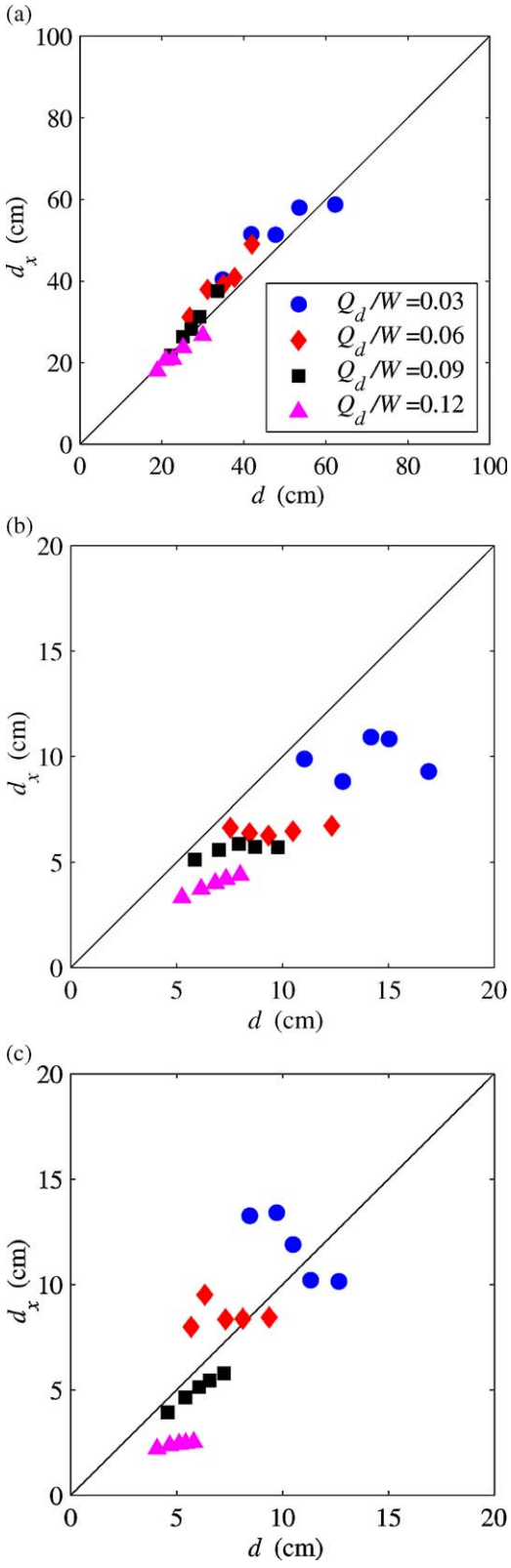

Fig. 7. Comparison of median maximum isolator displacements from unidirectional response-history analysis and maximum isolator displacements as per AASHTO: (a) Bin 1; (b) Bin 2M; (c) Bin 7.

isolator displacement for isolation systems with Q_d/W equal to 0.03 and 0.06 and $T_d < 3.0$ s. This underestimation is due to the frequency content of the ground motion components contained in Bin 7 causing a resonant effect for isolation systems with $Q_d/W \leq 0.06$ and $T_d \leq 2.5$ s.

4.3. Bidirectional response-history analysis

The results of bidirectional nonlinear response-history analysis were mined to determine maximum horizontal isolator displacements. Maximum horizontal isolator displacements were determined from the SRSS displacement response calculated at each time step during the response-history analysis. Median maximum horizontal isolator displacements, denoted d_{xy}, were computed for each isolation system and ground motion bin. Shown in Fig. 8 is a comparison of median maximum horizontal isolator displacements with the calculated AASHTO displacements. From Fig. 8a (Bin 1), the AASHTO calculated displacement is shown to underestimate the median maximum isolator displacement for all isolation systems considered by a factor (d_{xy}/d) of approximately 2.0. Fig. 8b shows the AASHTO calculated displacement for Bin 2M underestimate the median maximum horizontal isolator displacement for 13 of the 20 isolation systems by a maximum factor (d_{xy}/d) of 1.8. Fig. 8c shows the AASHTO calculated displacement underestimate median maximum horizontal isolator displacement for all isolation systems considered by a maximum factor (d_{xy}/d) of 3.0. This large difference is again due to the frequency content of the ground motion components contained in Bin 7 and occurred for an isolation system with $Q_d/W = 0.03$ and $T_d = 1.5$ s.

4.4. Displacement contribution factors

Bidirectional excitation is shown to result in maximum isolator displacements that are significantly larger than those considering unidirectional excitation only. Two factors contribute to the increased displacement, namely, a second (orthogonal) component of excitation and the coupled behavior of seismic isolators (demonstrated previously). The increase in maximum isolator displacement due to bidirectional excitation is defined as

$$\alpha_{xy}^{i} = \frac{d_{xy}^{i}}{d_{x}^{i}} \tag{8}$$

where d_{xy}^{i} is the maximum horizontal isolator displacement determined from bidirectional response-history analysis considering a circular yield surface (coupled); and d_{x}^{i} is the maximum isolator displacement determ-

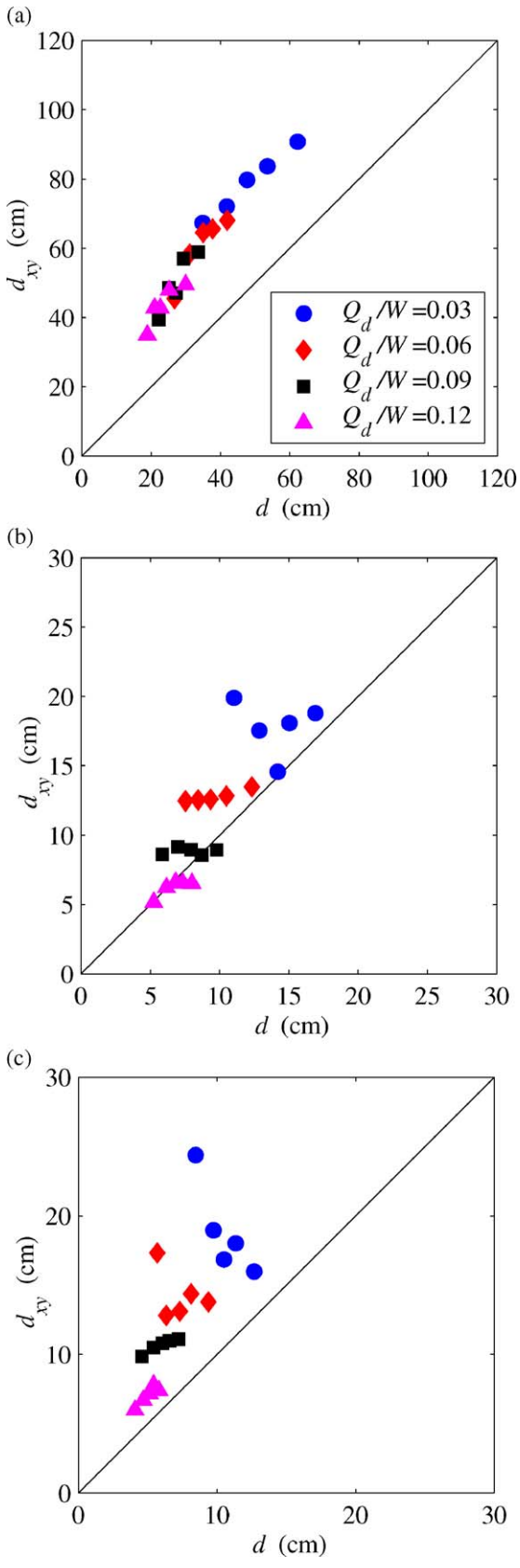

Fig. 8. Comparison of median maximum isolator displacements from bidirectional response-history analysis and maximum isolator displacements as per AASHTO: (a) Bin 1; (b) Bin 2M; (c) Bin 7.

ined from unidirectional response-history analysis using the 1st ground motion component of the ith ground motion pair. To identify the contribution from each factor, Eq. (8) was re-written as the product of two ratios

$$\alpha_{xy}^{i} = \left(\frac{\tilde{d}_{xy}^{i}}{d_{x}^{i}}\right)\left(\frac{d_{xy}^{i}}{\tilde{d}_{xy}^{i}}\right) \tag{9}$$

where $\tilde{d}_{xy}^{i}$ is the maximum horizontal isolator displacement determined from the SRSS response calculated from two independent unidirectional response-history analyses using the 1st and 2nd components of the ith ground motion pair, equivalent to bidirectional response-history analysis considering a square yield surface (uncoupled). For convenience, Eq. (9) is re-expressed as

$$\alpha_{xy}^{i} = \alpha_{o}^{i}\alpha_{c}^{i} \tag{10}$$

where α_{o}^{i} represents the contribution due to the second ground motion component and is equal to the ratio $\tilde{d}_{xy}^{i}/d_{x}^{i}$; and α_{c}^{i} represents the contribution due to the coupled behavior and is equal to the ratio $d_{xy}^{i}/\tilde{d}_{xy}^{i}$.

Values of α_{xy} and α_{o} were calculated for each isolation system and ground motion pair. Median values of α_{xy} and α_{o} are presented in Fig. 9. From Fig. 9a (Bin 1), values of α_{xy} are observed to range from 1.03 to 1.17 and values of α_{c} from 1.03 to 1.11. In Fig. 9b (Bin 2M), α_{xy} is observed to range from 1.3 to 1.8 and α_{c} from 1.06 to 1.2. In Fig. 9c (Bin 7), α_{xy} is observed to range from 1.2 to 2.4 and α_{c} from 1.05 to 1.5. The results shown in Fig. 9 suggest the following. The increase in displacement due to bidirectional excitation for ground motion pairs exhibiting directivity effects (Bin 1) is modest, on the order of 17%, and is mostly due to the coupling of the seismic isolator, suggesting that the second (smaller) component contributes little to the total response for this ground motion bin only. For ground motion pairs that exhibit null directivity effects (Bin 2M and Bin 7), both factors contribute significantly to maximum isolator displacement. For all ground motion bins considered, an increasing trend in α_{c} is observed for increasing Q_{d}/W.

5. Energy demands on seismic isolators

5.1. Normalized energy dissipated

Force–displacement response data determined from the results of unidirectional and bidirectional response-history analyses conducted in support of the maximum isolator displacement study were mined to determine energy-related demands imposed on seismic isolators during maximum earthquake excitation. For this study, the energy dissipation capacity of the isolators has been assumed to be equal to the energy demands imposed on the seismic isolators. The cumulative energy demand imposed on individual seismic isolators is determined by numerically integrating the force–displacement response. For bidirectional excitation, the total cumulative energy demand is calculated as the sum of the total energy in the x- and y-directions. For this study, the total cumulative energy has been normalized by the energy dissipated from one fully reversed cycle to the maximum displacement, determined from response-history analysis. Normalized energy dissipated (NED) is defined as

$$\text{NED} = \frac{\int F\ \mathrm{d}u}{\text{EDC}} \tag{11}$$

where F is the restoring force of the seismic isolator; du is an incremental displacement; and EDC is the energy dissipated from one fully reversed cycle to the maximum displacement, where the maximum isolator displacement is determined from response-history analysis. The EDC by a bilinear isolator (see Fig. 4) is calculated using Eq. (12) and was adopted from the AASHTO Guide Specifications [1]

$$\text{EDC} = 4Q_{d}(d_{\max} - d_{y}) \tag{12}$$

where $d_{\max}$ is the maximum isolator displacement; and d_{y} is the yield displacement assumed herein to be negligible. Normalizing the total energy dissipated by the EDC allows the results of this study to be generally applicable to isolators and isolation systems idealized using a bilinear force–displacement relationship and represents the number of harmonic cycles to the maximum displacement to dissipate an amount of energy equivalent to the total energy demand due to a severe earthquake.

Normalized energy dissipated statistics determined from the results of bidirectional response-history analysis using ground motion pairs from Bin 1 are shown in Fig. 10. In Fig. 10a, mean NED is plotted as a function of Q_{d}/W for each of the five values of T_{d} considered. Mean NED information including sample standard deviation information is reproduced for isolation systems with T_{d} equal to 2.0, 2.5 and 3.0 s in Figs. 10b,c and d, respectively. Sample standard deviation information has been plotted to indicate the dispersion of NED data about the mean. The results of NED calculated from bidirectional response-history analysis using ground motion pairs from Bin 2M and Bin 7 are shown in Figs. 11 and 12, respectively. The presentation used for Figs. 11 and 12 is the same as Fig. 10. Similar trends in mean NED are observed for all three ground motion bins, namely, decreasing NED

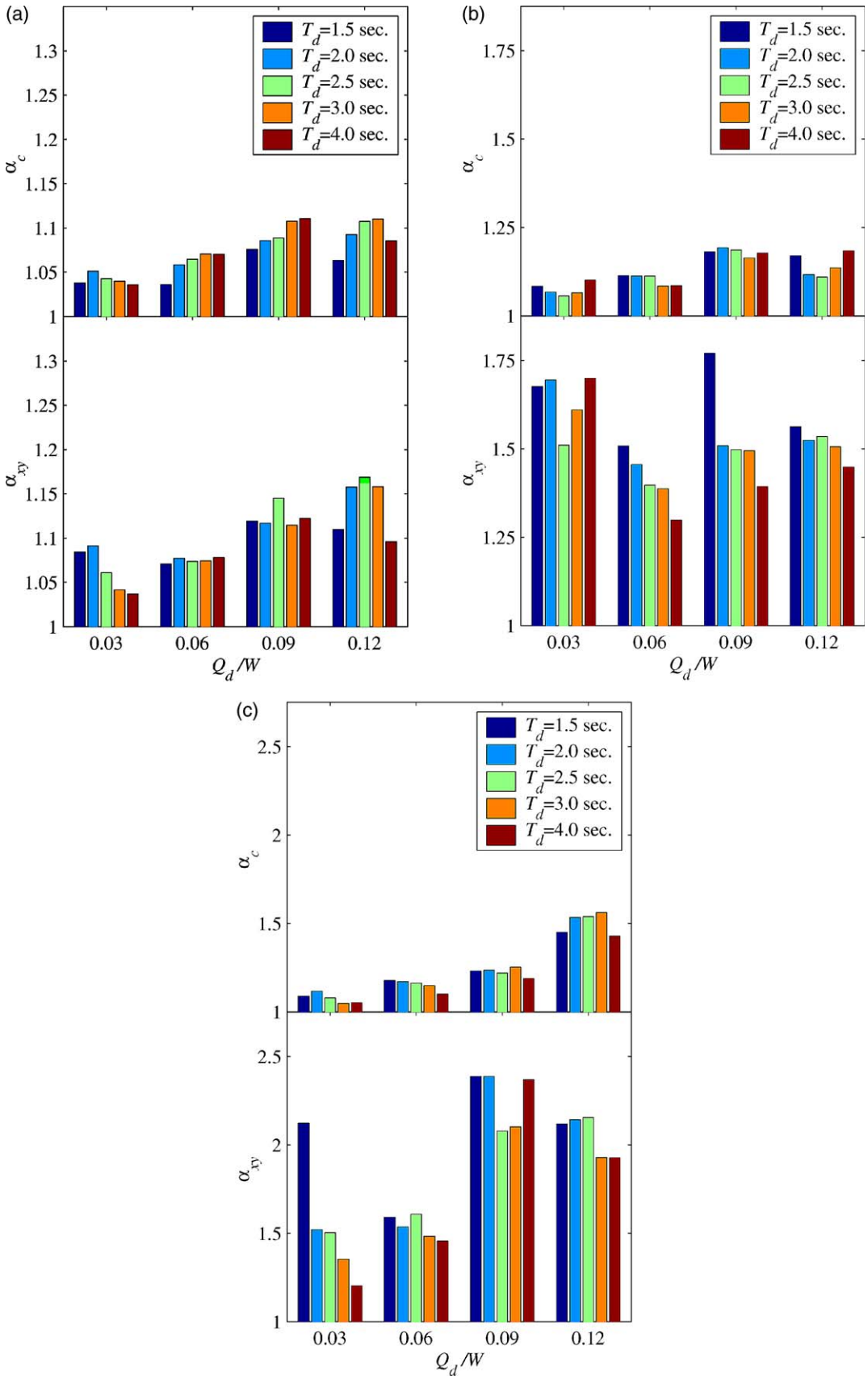

Fig. 9. Median increase in displacement due to bidirection excitation and coupling in seismic isolators: (a) Bin 1; (b) Bin 2M; (c) Bin 7.

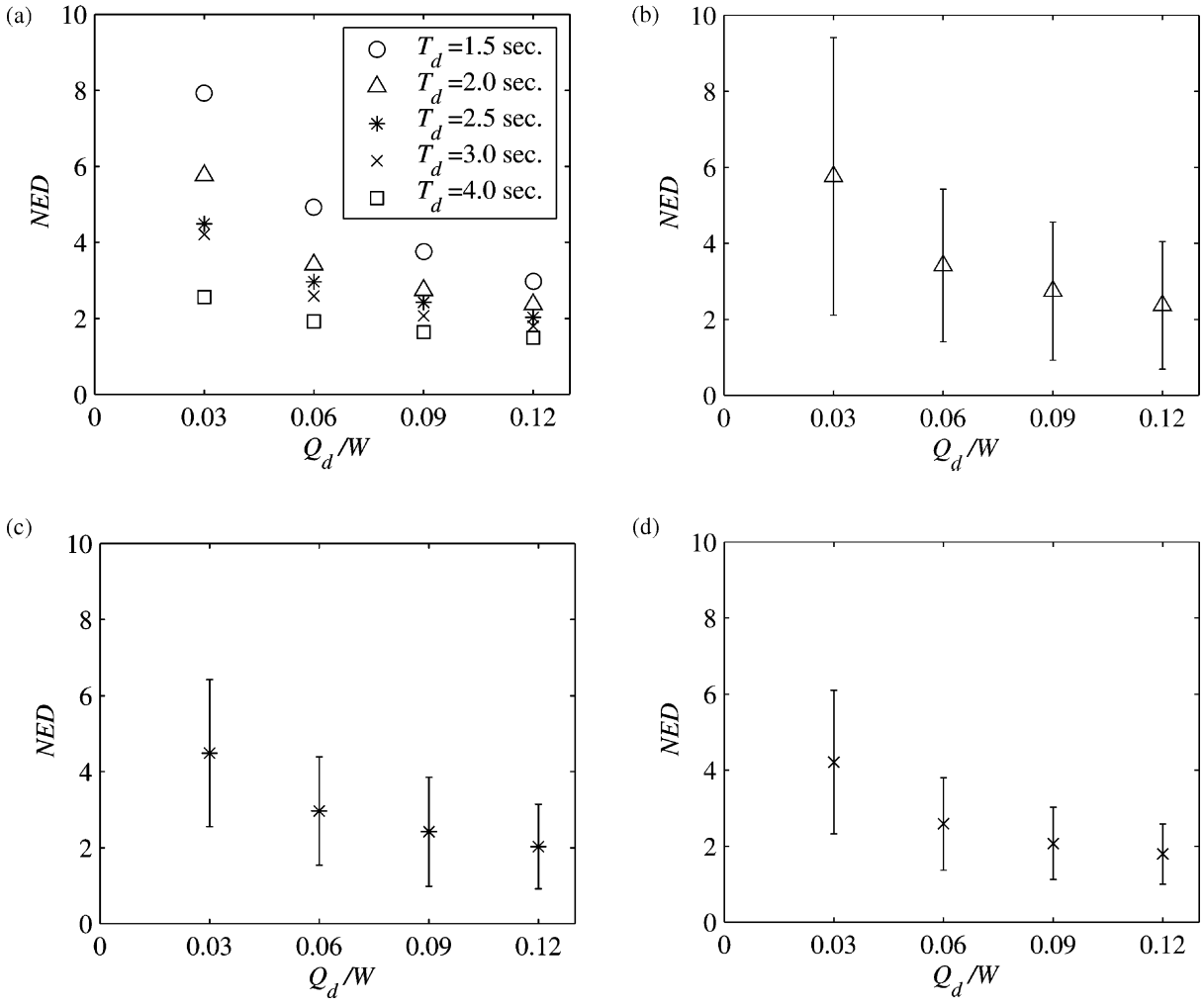

Fig. 10. Normalized energy dissipated considering bidirectional excitation using Bin 1 ground motion pairs: (a) mean; (b) mean $\pm 1\sigma$ for $T_d = 2.0$ s; (c) mean $\pm 1\sigma$ for $T_d = 2.5$ s; (d) mean $\pm 1\sigma$ for $T_d = 3.0$ s.

with increasing Q_d/W and increasing T_d. Mean and mean $+ 1\sigma$ NED data calculated for Bins 1, 2M and 7 are re-plotted for all isolation systems with $T_d = 2.0$ s in Fig. 13. From Fig. 13a, it is observed that NED = 4.0 (four fully reversed cycles to the maximum displacement) conservatively estimates mean total energy demands for isolation systems with $Q_d/W \geq 0.06$ (typical of bridge applications). Considering the same isolation systems, NED = 5.0 is observed to reasonably estimate the mean $+ 1\sigma$ energy demands for each ground motion bin shown in Fig. 13b.

5.2. Power demand

The power demand placed on seismic isolators during earthquake excitation is estimated from energy histories calculated from the results of unidirectional and bidirectional response-history analysis. Power (or energy rate) estimates were calculated for each isolation system and ground motion pair using

$$R_E^{50} = \frac{0.75E_T - 0.25E_T}{t_{75} - t_{25}} \tag{13}$$

where R_E^{50} is the estimated power based on a 50% range of the total energy; E_T is the total energy; t_{25} is the time coinciding with 25% of the total cumulative energy; and t_{75} is the time coinciding with 75% of the total cumulative energy. Fig. 14 shows a simple schematic of the power definition employed for this study. The energy history used in this figure is from the results of unidirectional response-history analysis using ground motion component RIO360 (included in Bin 2M) with isolator properties: $Q_d/W = 0.06$ and $T_d = 2.5$ s.

An equivalent harmonic frequency is calculated using estimates of the power demand placed on individual seismic isolators (R_E^{50}). This equivalent harmonic frequency is used to determine an appropriate fre-

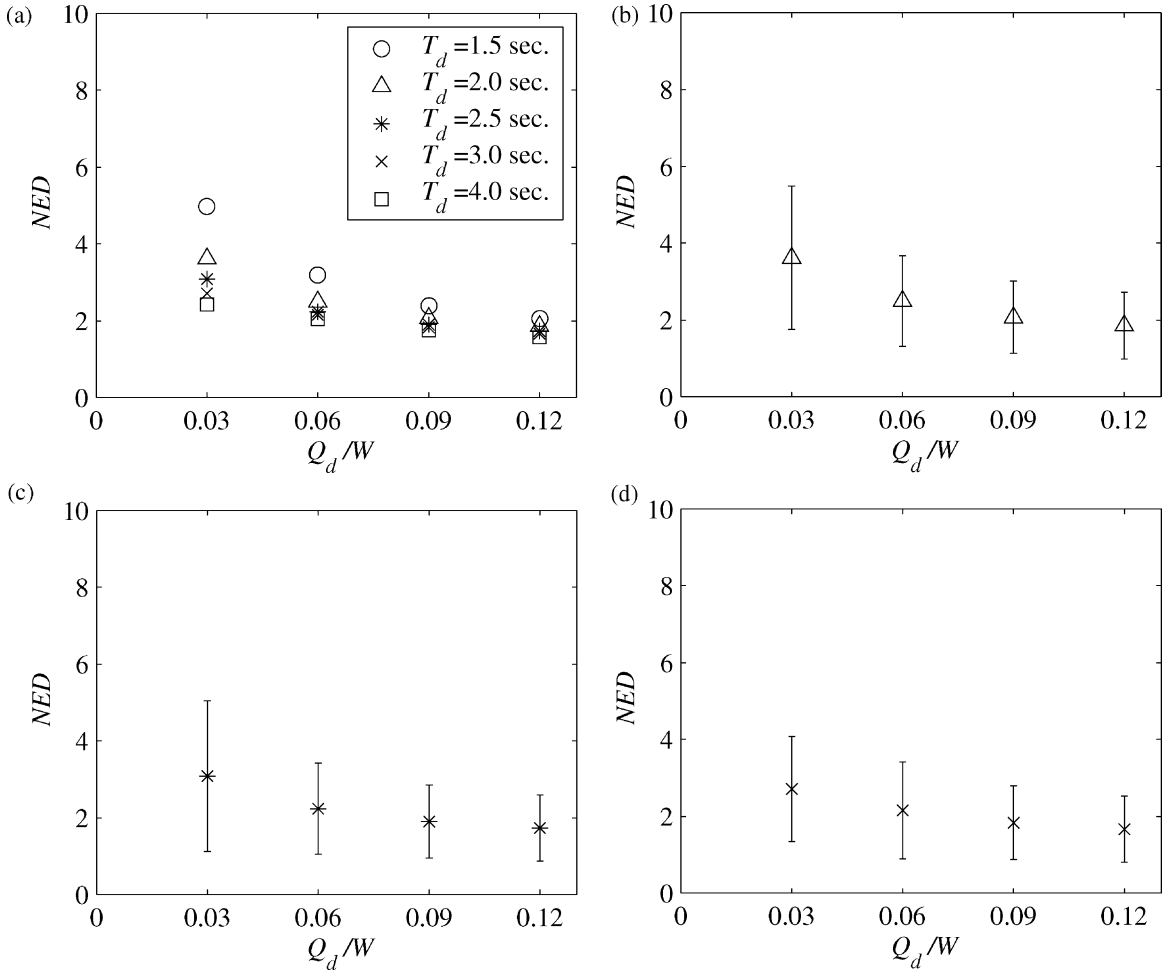

Fig. 11. Normalized energy dissipated considering bidirectional excitation using Bin 2M ground motion pairs: (a) mean; (b) mean $\pm 1\sigma$ for $T_d = 2.0$ s; (c) mean $\pm 1\sigma$ for $T_d = 2.5$ s; (d) mean $\pm 1\sigma$ for $T_d = 3.0$ s.

quency for prototype testing of seismic isolators. The equivalent harmonic frequency is calculated as

$$f_{\text{eq}} = \frac{R_E^{50}}{\text{EDC}} \tag{14}$$

where EDC is the energy dissipated from one fully reversed cycle of displacement to the maximum displacement calculated using Eq. (12). Sample results of the equivalent harmonic frequency calculated from the results of unidirectional response-history analysis using ground motion component RIO360 for three isolation systems are shown in Table 5. Also presented in Table 5 is a frequency calculated from the effective period of the isolation system, denoted $1/T_{\text{eff}}$, where T_{eff} is the effective period of the isolation system at the maximum displacement calculated using the effective stiffness, K_{eff} (see Fig. 4). The results of the calculated equivalent harmonic frequency shown in Table 5 suggest that use of the effective period, T_{eff}, results in a harmonic frequency that reasonably estimates the power demand placed on seismic isolators during earthquake excitation. Note that $1/T_{\text{eff}}$ (Column 11 of Table 5) leads to a slightly unconservative estimate of f_{eq} (Column 10 of Table 5) for the isolation system with $Q_d/W = 0.12$ and $T_d = 3.0$ s.

6. Summary and conclusions

The design of seismic isolation systems for bridge structures in the United States is governed by the AASHTO Guide Specifications for Seismic Isolation Design [1]. These specifications proved procedures for the design and analysis of individual seismic isolators and isolation systems, and procedures for full-scale testing of seismic isolators. This study aimed to: (1) review the accuracy of Eq. (3) of the Uniform Load Method in the Guide Specification for the calculation of maximum displacements in seismic isolation systems, (2) investigate the contributing factors effecting maximum horizontal isolator displacement, namely, the second (orthogonal) component of ground motion and the coupled behavior of seismic isolators (F, LR and FP), and

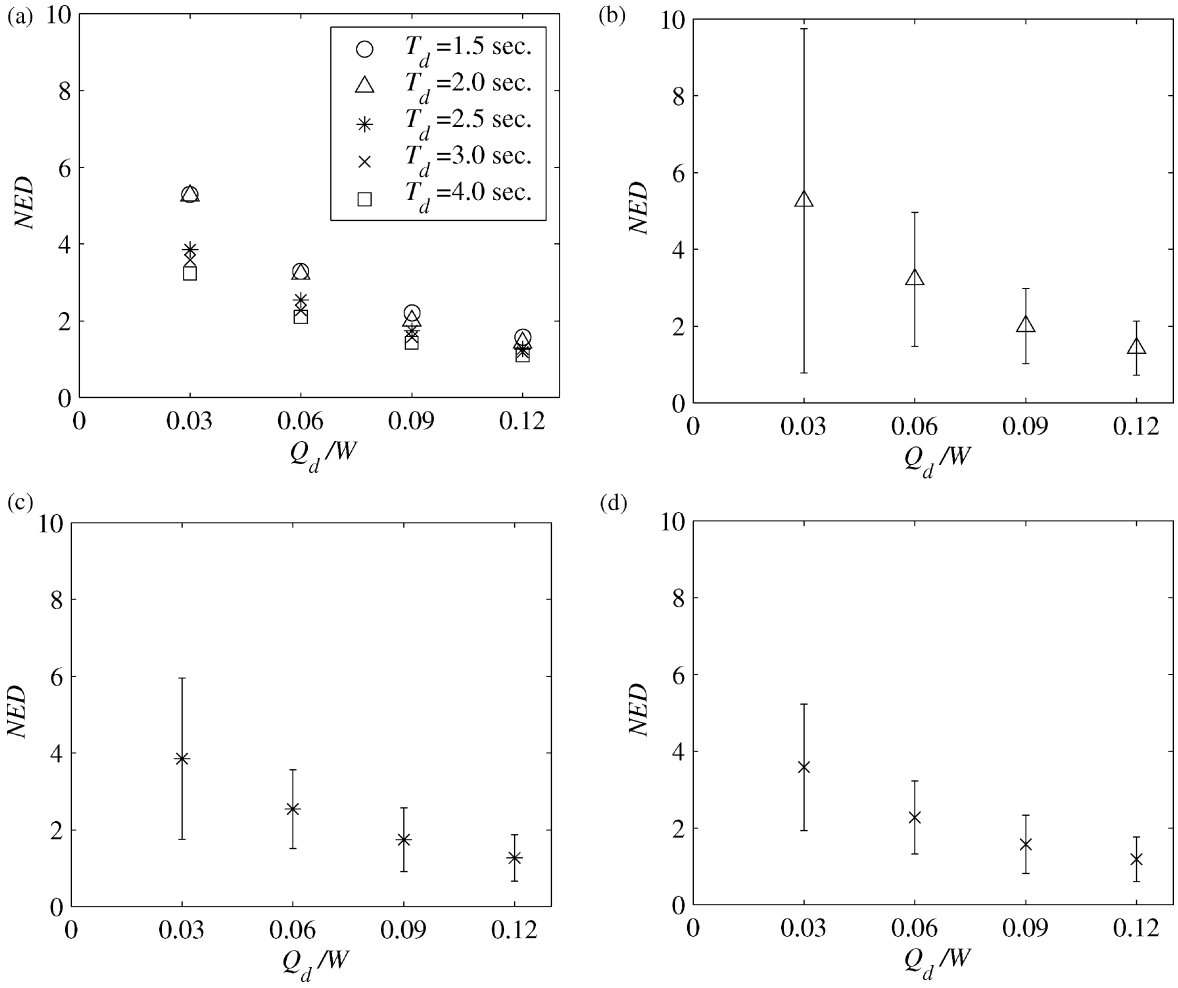

Fig. 12. Normalized energy dissipated for bidirectional excitation using Bin 7 ground motion pairs: (a) mean; (b) mean $\pm 1\sigma$ for $T_d = 2.0$ s; (c) mean $\pm 1\sigma$ for $T_d = 2.5$ s; (d) mean $\pm 1\sigma$ for $T_d = 3.0$ s.

(3) provide new information regarding energy demands imposed on individual seismic isolators and isolation systems subjected to earthquake excitation.

The results of this study show the current AASHTO equation underestimates median maximum horizontal isolator displacements despite the use of conservative (small) values of the damping coefficient and assumed linearly increasing displacements for periods greater than 1 s. Both the second component of excitation and the coupled behavior contribute significantly to maximum horizontal isolator displacements with the exception of Bin 1 where the second component was observed to contribute little. Results of the investigation of energy demands imposed on seismic isolators suggest the current AASHTO prototype testing protocol for seismic loading is inconsistent with the energy demands observed from numerical simulation of maximum earthquake excitation. Further conclusions of this study are:

(1) Maximum isolator displacements calculated using Eq. (3) of the AASHTO Guide Specifications were shown to estimate median maximum isolator displacements determined from unidirectional response-history analysis with reasonable accuracy for Bin 1 and conservatively estimate median maximum isolator displacements considering ground motion Bin 2M with site soil conditions corresponding to rock and stiff-soil sites, respectively. For Bin 7, the AASHTO calculated displacement conservatively estimated median maximum isolator displacements for isolation systems with $Q_d/W \geq 0.09$ and underestimated median maximum isolator displacements for most isolation systems with $Q_d/W \leq 0.06$.

(2) The AASHTO isolator displacement equation underestimates maximum isolator displacements determined from bidirectional response-history analysis for all isolation systems, considering ground motion Bins 1 and 7, and for 13 of 20 isolation systems for ground motion Bin 2M because (i) the coupled response of the seismic isolators is not considered in the AASHTO calculation that was shown to be significant for all ground motion

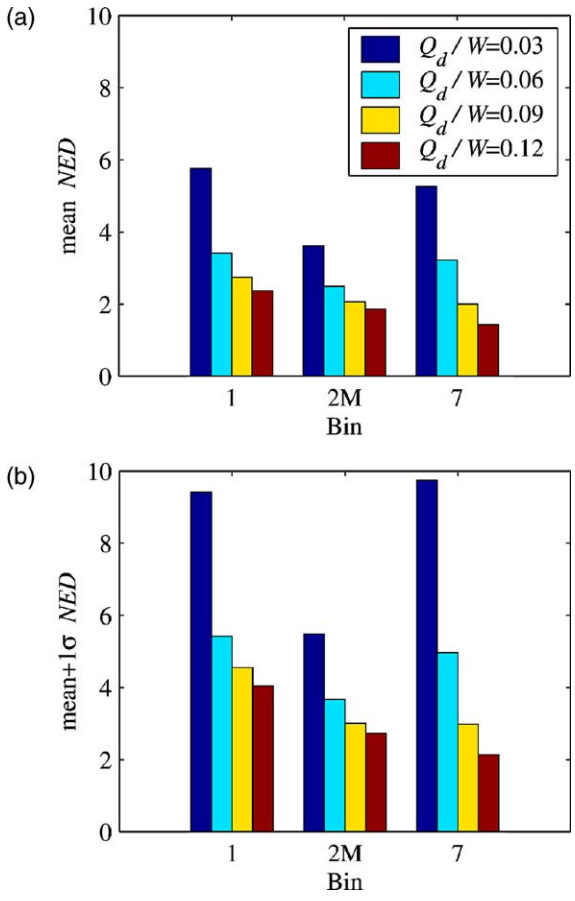

Fig. 13. Normalized energy dissipated statistics for ground motion Bins 1, 2M, and 7 for isolation systems with $T_d = 2.0$ s: (a) mean; (b) mean $\pm 1\sigma$.

bins; (ii) for Bin 1 (near-field), the AASHTO calculated displacement systematically underestimates maximum isolator displacements because the hazard is not characterized by the fault normal component; (iii) for Bins 2M and 7, the AASHTO calculation does not account for the significant contribution from a second (orthogonal) component of excitation; and (iv) for Bin 7 (soft-soil), the current characterization of the hazard may not accurately represent seismic demands on long-period structures such as isolation systems.

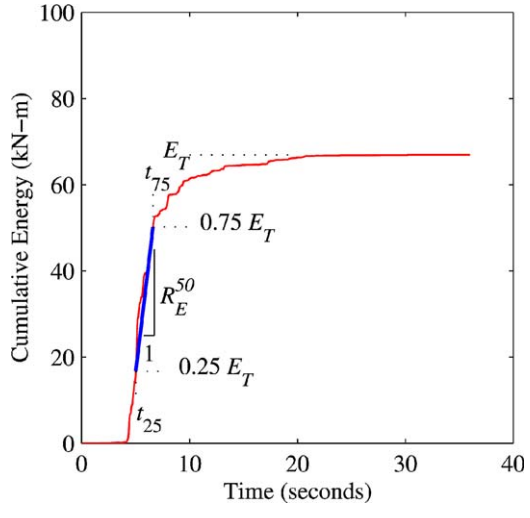

Fig. 14. Sample energy history determined from unidirectional response-history analysis considering an isolation system with $Q_d/W = 0.06$ and $T_d = 2.0$ s using ground motion component RIO360.

(3) The second (orthogonal) component of excitation appears to contribute to the maximum horizontal isolator displacement significantly, with the exception of Bin 1 (near-field) where the second (fault parallel) component contributed little to the maximum horizontal isolator displacement. Ongoing research will quantify the contribution from the orthogonal component of motion and propose a factor, α_o, as part of the new equation for calculating displacements in seismically isolated bridge structures.

(4) The coupled response (circular yield surface) is shown to contribute significantly to the maximum horizontal isolator displacement for all ground motion bins considered. The results of this study suggest a value of α_c equal to 1.2 conservatively estimates the increase in displacement due to coupling for all ground motion bins and isolation system with the exception of Bin 7 and isolation systems with $Q_d/W = 0.12$ where α_c was greater than 1.2.

(5) Energy demands, in terms of total cumulative energy, imposed on seismic isolators determined from numerical simulation of maximum earthquake excitation are far less than the energy demands imposed on seismic isolators from the current AASHTO prototype testing protocol for seismic isolators subjected to seismic loading. The current testing protocol calls for 22 cycles to a displacement equal to or greater than the design displacement and 31 cycles of displacement to various amplitudes typically conducted as low maximum velocities.

The following recommendations are provided based on the results of this study:

(1) The coupled response of seismic isolators and the additional displacement demand from a second (orthogonal) component of excitation should be considered in the AASHTO equation for calculation displacements in seismically isolated bridge structures.

(2) For isolated bridge structures constructed in close proximity to major active seismic faults, the design spectrum must include directivity effects.

(3) For isolated bridge structures constructed on soft-soil (e.g. NEHRP site class E and F or USGS site class D), nonlinear response-history analysis must

Table 5
Sample results of the equivalent harmonic frequency calculated from the results of unidirectional response-history analysis using ground motion component RIO360

Q_d/W	T_d (s)	W (kN)	g (m/s^2)	K_d (kN/m)	R_E 50 (kN m/s)	d_{max} (cm)	K_{eff} (kN/m)	T_{eff} (s)	f_{eff} (Hz)	$1/T_{eff}$ (Hz)
0.06	2.0	2473	9.81	2488	22.3	6.4	4795	1.44	0.58	0.69
0.09	2.5			1592	29.0	5.8	5400	1.36	0.56	0.74
0.12	3.0			1106	58.6	5.7	6304	1.26	0.86	0.80

be employed to confirm displacement demands on long-period (isolated) structures.

(4) An improved prototype testing protocol for seismic isolators subjected to seismic loading include: four fully reversed cycles to the total design displacement at a frequency equal to $1/T$, where the total design displacement includes the maximum isolator displacement plus a provision for an increase due to torsion and T is the effective period of the isolated structure.

Acknowledgements

The authors gratefully acknowledge the financial support of the Multidisciplinary Center for Earthquake Engineering Research and the Federal Highway Administration through Task D1.3 of the Federal Highway Administration Contract DTFH 61-98-C-0094. The authors also wish to thank Professor Eduardo Miranda of Stanford University for contributing ground motion records for use in this study and Dr. Gilberto Mosqueda of the University of California at Berkeley for providing the Matlab code for the coupled plasticity model.

The opinions expressed in this paper are those of the writers and do not reflect the opinions of the Multidisciplinary Center for Earthquake Engineering Research or the Federal Highway Administration. No guarantee regarding the results, findings, and recommendations are offered by either the Multidisciplinary Center of Earthquake Engineering Research or the Federal Highway Administration.

References

[1] American Association of State Highway Officials. Guide specifications for seismic isolation design. Washington (DC): American Association of State Highway Officials; 1999.

[2] American Association of State Highway Officials. Standard specifications for highway bridges, 16th ed. Washington (DC): American Association of State Highway Officials; 1996.

[3] Mokha AS, Constantinou MC, Reinhorn AM. Verification of friction model of Teflon bearings under triaxial load. Journal of Structural Engineering, ASCE 1993;119(1):240–61.

[4] Huang WH, Fenves GL, Whittaker AS, Mahin SA. Characterization of seismic isolation bearings for bridges from bi-directional testing. Proceedings of the 12th World Conference on Earthquake Engineering. 2000, p. 2047–8.

[5] Mosqueda G, Whittaker AS, Fenves GL. Characterization and modeling of friction pendulum bearings subjected to multiple components of excitation. Journal of Structural Engineering, ASCE, 2004;130(3):433–42.

[6] Krawinkler H. Personal communication, 2001.

[7] Warn G. Performance estimates in seismically isolated bridge structures. M.S. Thesis, University at Buffalo, NY, 2003.

[8] Pacific Earthquake Engineering Research. Strong motion database, 2000. Available from: http://peer.berkeley.edu/smcat/.

[9] SAC Steel Project. Suites of earthquake ground motions for analysis of steel moment frame structures, 1997. Available from: http://nisee.berkeley.edu/data/strong_motion/sacsteel/ground_motions.html.

[10] Miranda E. Personal communication, 2002.

[11] National Earthquake Hazard Reduction Program. Recommended provisions for seismic regulations for new buildings and other structures, Part-1. Washington (DC): Building Seismic Safety Council for the Federal Emergency Management Agency; 2001.

[12] Benuska L. Loma Prieta earthquake reconnaissance report. Earthquake Spectra 1990;6(Suppl):25–80.

[13] Miranda E. Seismic evaluation and upgrading of existing buildings. Ph.D. Thesis, University of California, Berkeley, CA, 1991.

[14] Youd TL, Bardet JP, Bray JD. Kocaeli, Turkey, earthquake of August 17, 1999 reconnaissance report. Earthquake Spectra 2000;16(Suppl):65–6.

[15] Applied Technology Council. Seismic design guidelines for highway bridges. Report 6. Redwood City, CA, 1986.

[16] Newmark NM. A method of computation for structural dynamics. Journal of the Engineering Mechanics Division ASCE 1959;85(3):67–94.

[17] MathWorks. Matlab. Natick (MA): The Math Works, Inc; 1999.

[18] Computers and Structures. SAP2000 nonlinear version 7.4: structural analysis program. Berkeley, CA: Computers and Structures, Inc; 2000.